SUPPLEMENTARY INFORMATION

Ruthenium-nickel heterobimetallic complex as a bifunctional catalyst for ROMP of norbornene and ethylene polymerization

Gustavo H. C. Masson[a], Thaís R. Cruz[a], Patrik D. S. Gois[a], Daniele M. Martins[b], Benedito, S. Lima-Neto[b] , Guedmiller S. Oliveira[c], Antonio E. H. Machado[c], Katia Bernardo-Gusmão[d], Beatriz E. Goi[a], Valdemiro P. Carvalho-Jr[a*]

[a]*Faculdade de Ciências e Tecnologia, UNESP – Univ. Estadual Paulista, CEP 19060-900, Presidente Prudente, SP, Brazil*

[b]*Instituto de Química de São Carlos, Universidade de São Paulo, CEP 13560-970, São Carlos, SP, Brazil*

[c]*Instituto de Química, Universidade Federal de Uberlândia, P.O. Box 593, CEP 38400-089, Uberlândia, MG, Brazil*

[d]*Instituto de Química, Universidade Federal do Rio Grande do Sul, P.O. Box 15003, CEP 91501-970, Porto Alegre, RS, Brazil*

Correspondence to: Valdemiro P. Carvalho-Jr (E-mail: *valdemiro.carvalho@unesp.br*)

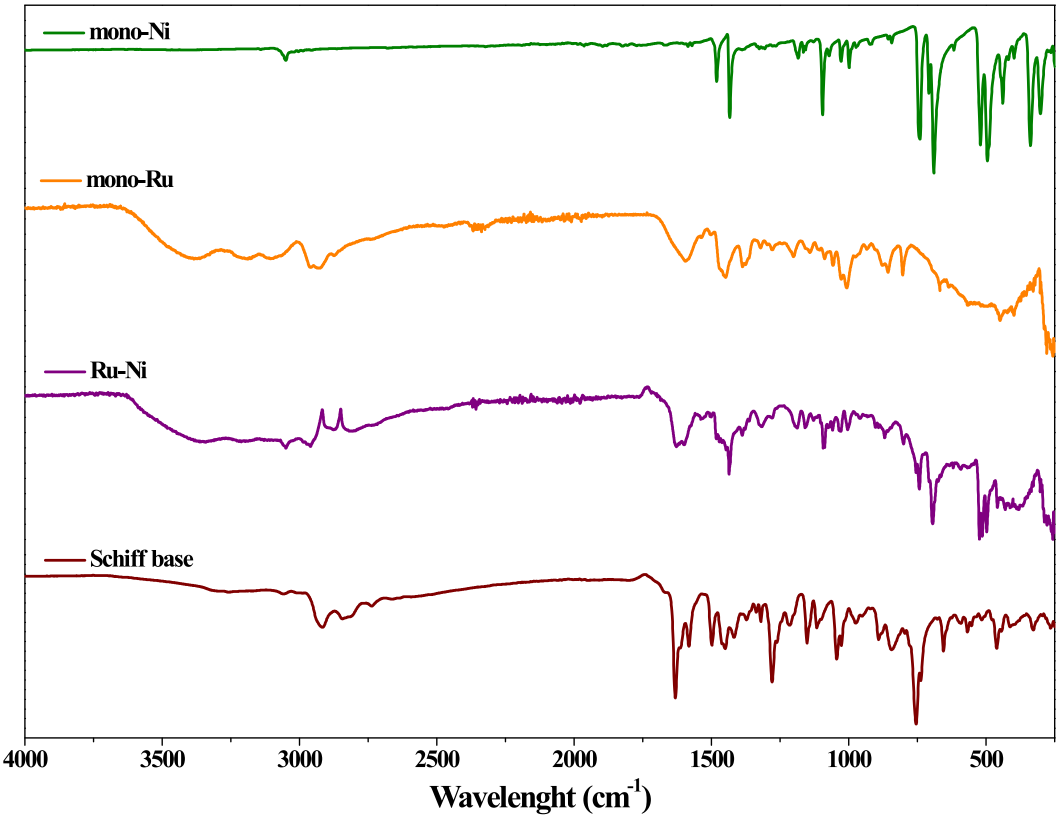

Fig. S1. FTIR spectra of Schiff base, **mono-Ru**, **mono-Ni**, and **Ru-Ni**.

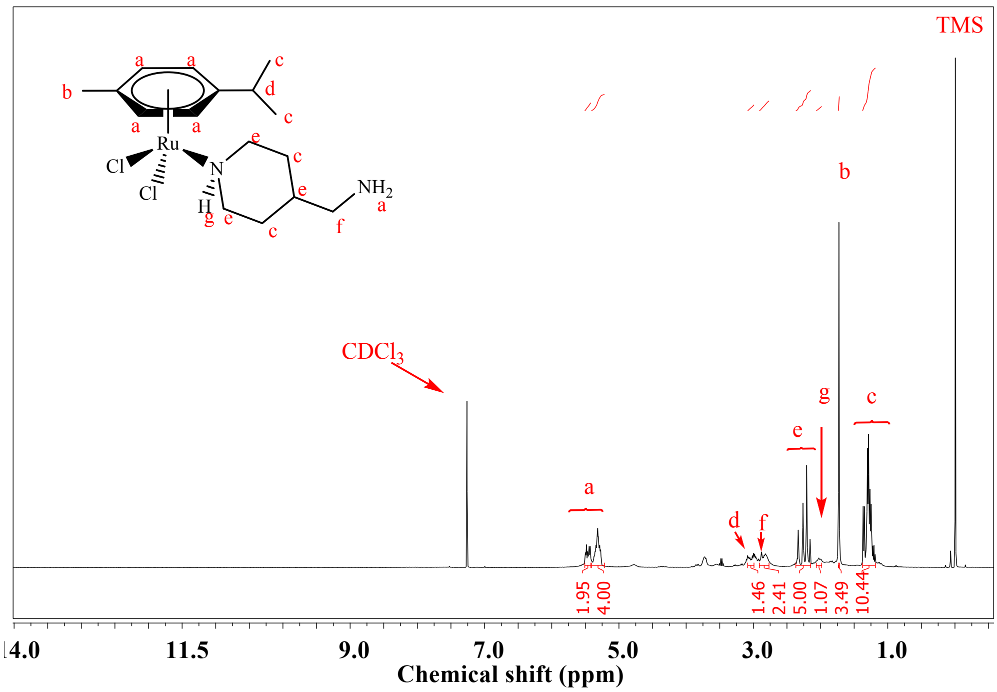

Fig. S2. ^{1}H NMR spectra of **mono-Ru** from $CDCl_3$ solutions (δ in ppm).

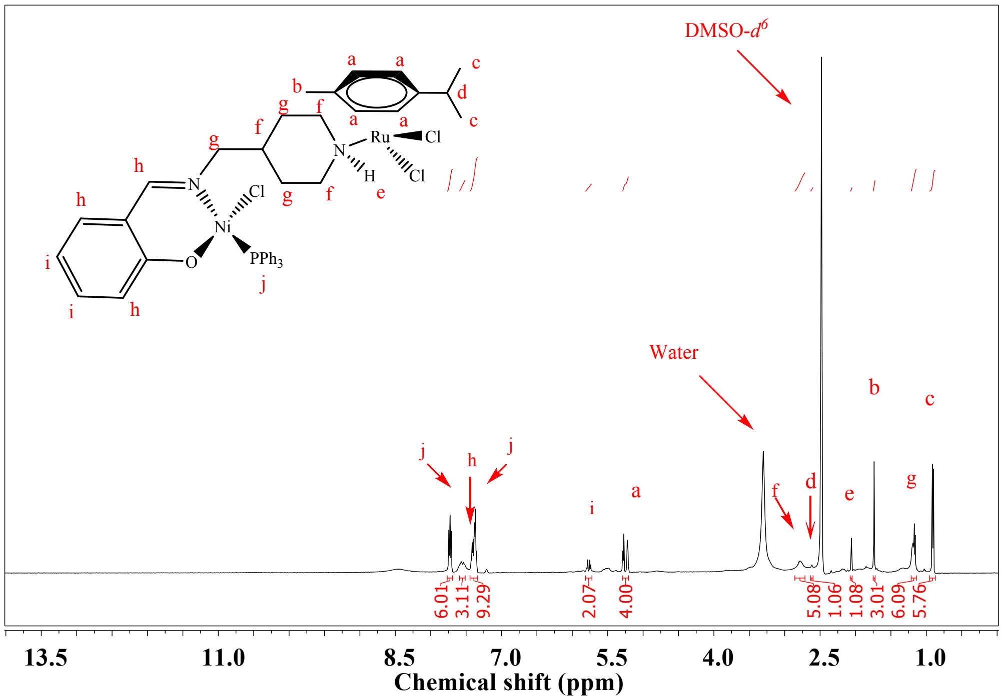

Fig. S3. ^{1}H NMR spectra of **Ru-Ni** from DMSO-*d*^{6} solutions (δ in ppm).

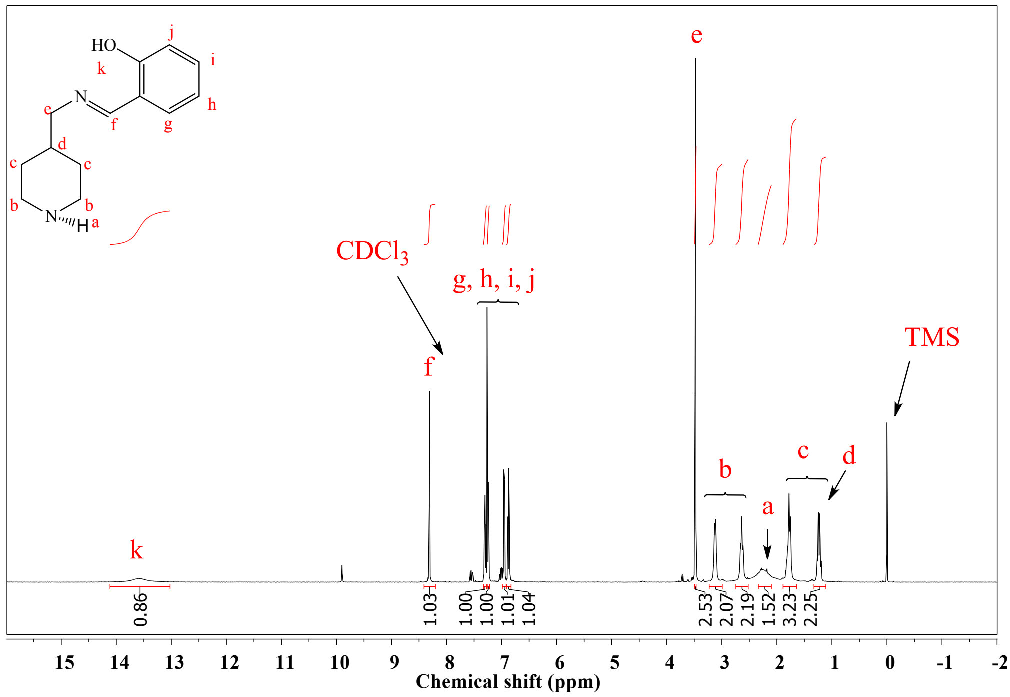

Fig. S4. ^{1}H NMR spectra of Schiff-pip from $CDCl_3$ solutions (δ in ppm).

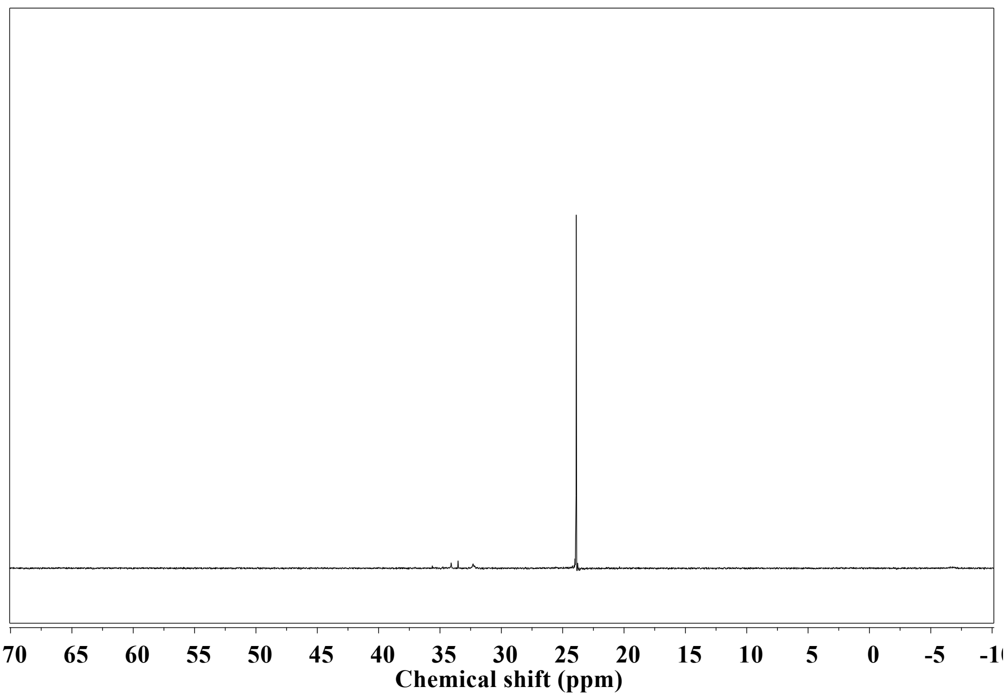

Fig. S5. ^{31}P {H} NMR spectra of **Ru-Ni** from DMSO-d^6 solutions (δ in ppm).

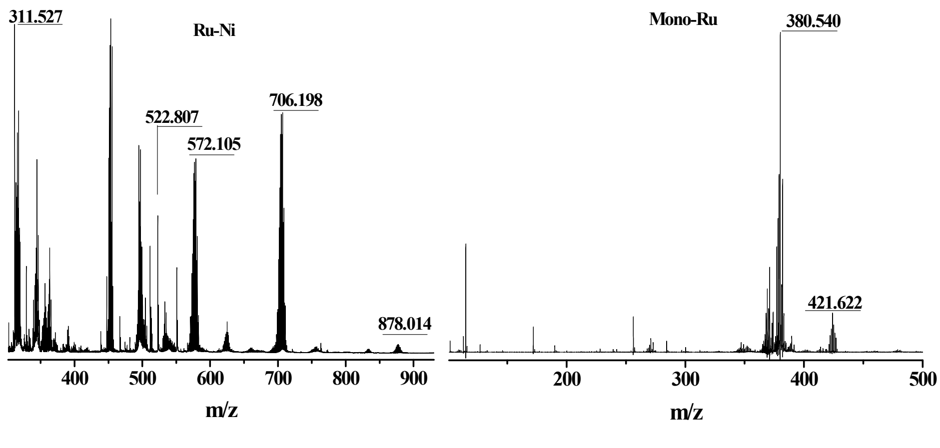

Fig. S6. MALDI-TOF spectrum of **Ru-Ni** and **mono-Ru** in MeOH.

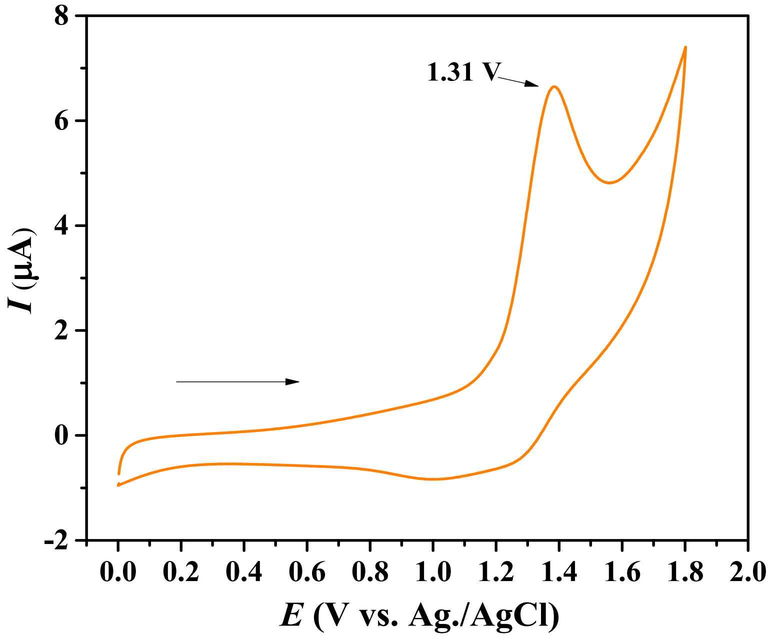

Fig. S7. Cyclic voltammogram of **mono-Ru** at $1.0{\cdot}10^{-3}$ M and *n*-Bu_4NPF_6/CH_2Cl_2 0.1 M *vs.* Ag/AgCl; obtained at 100 $mV{\cdot}s^{-1}$.

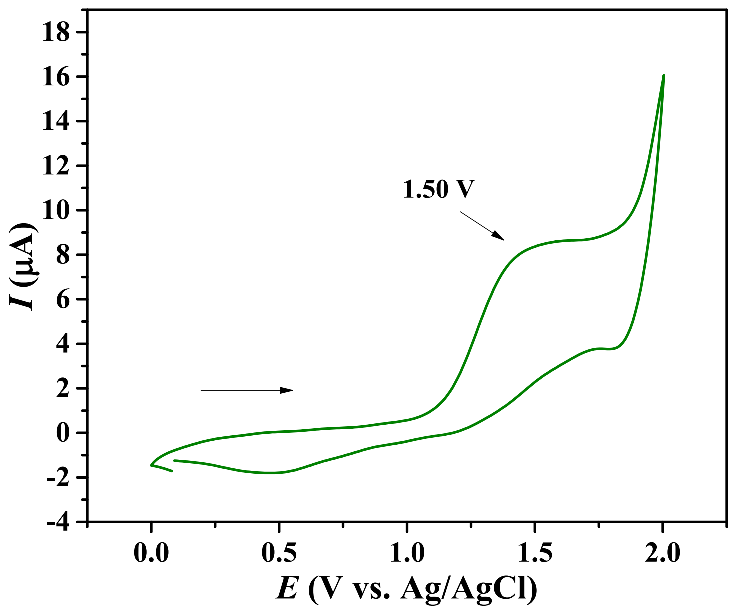

Fig. S8. Cyclic voltammogram of **mono-Ni** at $1.0{\cdot}10^{-3}$ M and *n*-Bu_4NPF_6/CH_2Cl_2 0.1 M *vs.* Ag/AgCl; scanning anodically from 0.8 up to 1.6 V at 100 $mV{\cdot}s^{-1}$.

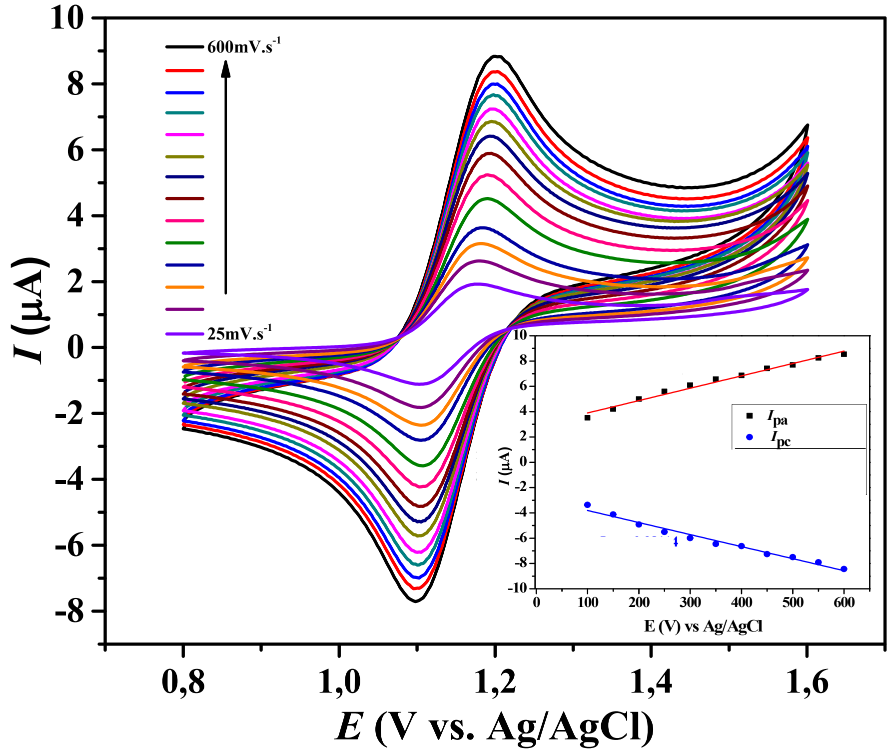

Fig. S9. Cyclic voltammogram of **Ru-Ni** at $1.0 \cdot 10^{-3}$ M and *n*-Bu_4NPF_6/CH_2Cl_2 0.1 M *vs.* Ag/AgCl; scanning anodically from 0.8 up to 1.6 V at scan rates of 25, 50, 75, 100, 150, 175, 200, 300, 400 and 500 mV s^{-1}. *Insert* - Current (*I*) of the anodic (I_{pa}) and cathodic (I_{pc}) processes vs. square root of the potential scan rate (v).

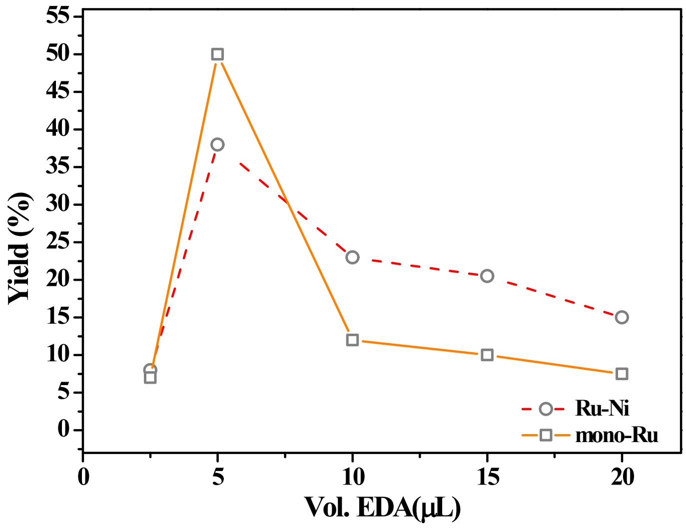

Fig S10. Dependence of yield as a function of the volume of EDA molar ratio for ROMP of NBE with **mono-Ru** and **Ru-Ni**; [NBE]/[Ru] = 5000 in $CHCl_3$ for 60 min.

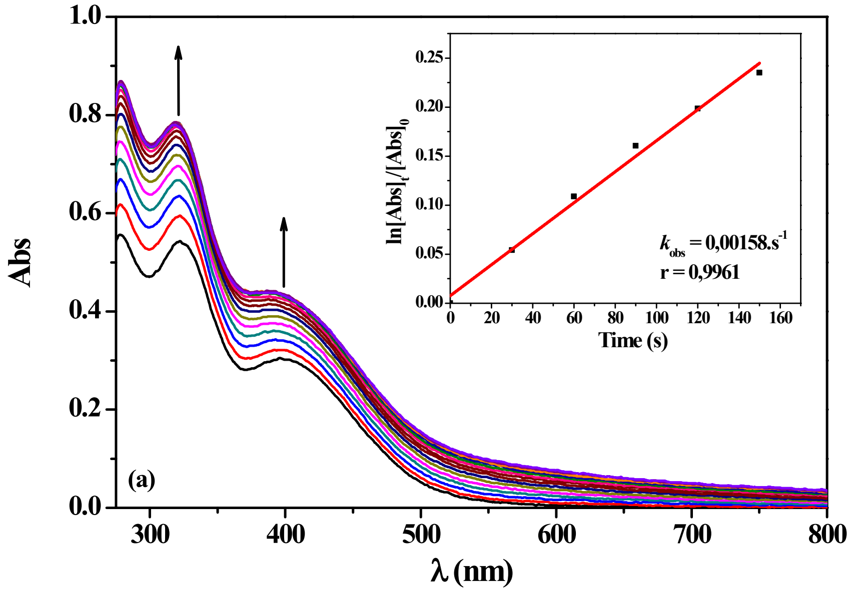

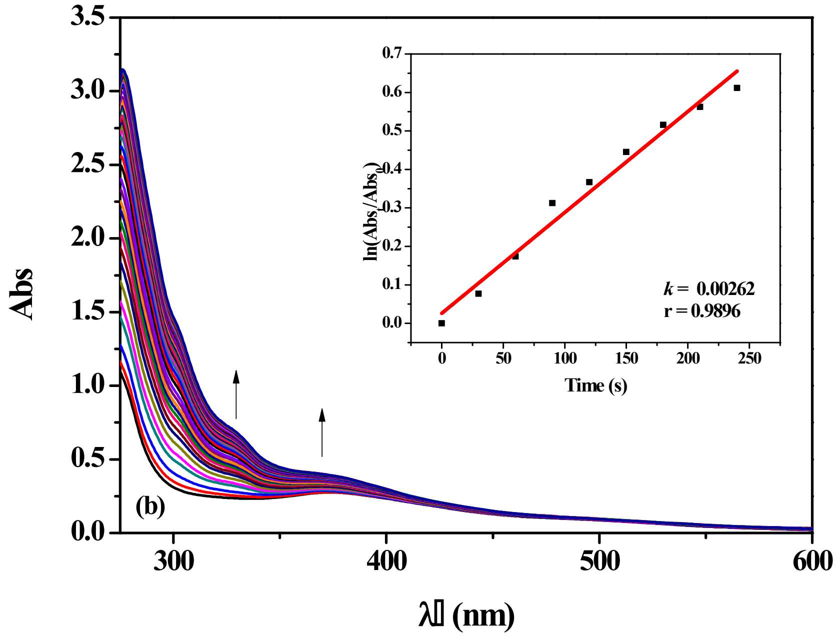

Fig. S11. Kinetic study of **mono-Ru** (a) and **Ru-Ni** (b) in presence of EDA monitored by electronic spectroscopy every 30 seconds and (*insert*) dependence of $\ln(Abs_t/Abs_0)$ as a function of time at 316 nm. [Ru] = $1.0 \cdot 10^{-5}$ M; [EDA] = $1.26 \cdot 10^{-5}$ mol L^{-1} in $CHCl_3$ and 25 ºC.

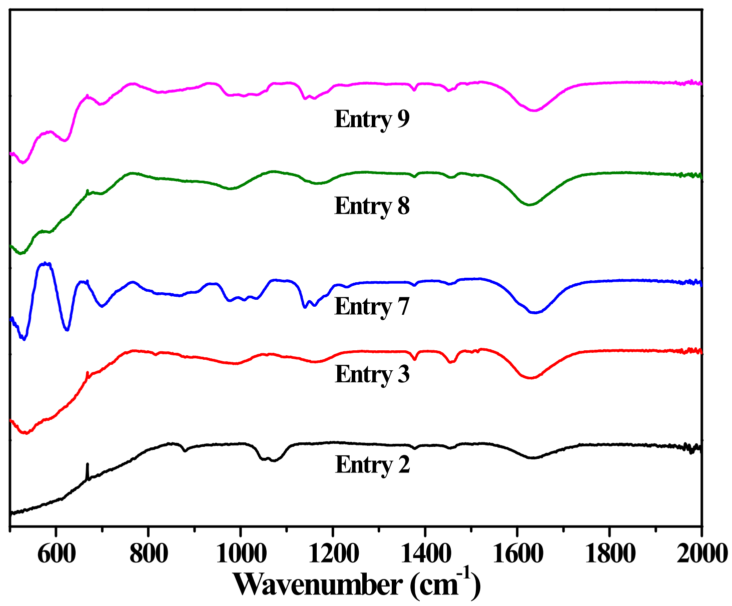

Fig. S12 FTIR spectra of polyethylene obtained from **Ru-Ni**.

Table S1 Peaks detected in the positive ion MALDI-TOF mass spectrum of the **Ru-Ni** and **mono-Ru** complex.

	Peak position (m/z)	m/z range	Peak assignment
Ru-Ni	311.527	309.528-320.575	[NiCl-(N,O)-(4-aminomethyl)]$^+$
	522.807	521.363-524.617	[RuCl$_2$(*p*-cymene)-(N,O)-(4-aminomethyl)]$^+$
	572.105	570.192-583.116	[Ni(PPh$_3$)Cl(N,O)-(4-aminomethyl)]$^+$
	706.198	696.905-712.930	[RuCl$_2$(μ-Schiff-pip)Ni(PPh$_3$)]$^+$
	878.014	869.625-883.558	[Ru-Ni+H+]$^+$
Mono-Ru	421.622	421.622-428.663	[Mono-Ru+H+]$^+$
	380.540	377.521-383.562	[RuCl$_2$(η^6-*p*-cymene)(pipNH$_2$)]$^+$-isopropyl